Soft Matter

PAPER

View Article Online
View Journal | View Issue

Cite this: *Soft Matter*, 2022, **18**, 4220

Linking cavitation and fracture to molecular scale structural damage of model networks†

Christopher W. Barney, ‡ Ipek Sacligil, Gregory N. Tew and Alfred J. Crosby *

Received 29th March 2022,
Accepted 16th May 2022

DOI: 10.1039/d2sm00400c

rsc.li/soft-matter-journal

Rapid expansion of soft solids subjected to a negative hydrostatic stress can occur through cavitation or fracture. Understanding how these two mechanisms relate to a material's molecular structure is important to applications in materials characterization, adhesive design, and tissue damage. Here, a recently improved needle-induced cavitation (NIC) protocol is applied to a set of model end-linked PEG gels with quantitatively linked elastic and fracture properties. This quantitative link between molecular scale structure and macroscopic properties is exploited to experimentally probe the relationship between cavitation, fracture, and molecular scale damage. This work indicates that rational tuning of the elastofracture length relative to the crack geometry can be used to alter the expansion mechanism from cavitation to fracture during NIC.

1 Introduction

Cavitation rheology encompasses a developing suite of techniques that exploit the phenomenon of cavitation to characterize the mechanical properties of soft gels and biological tissues.[1] Here cavitation is defined as the sudden, unstable expansion of a void or bubble in a fluid or solid subjected to negative hydrostatic stress. Needle-induced cavitation (NIC) is an important cavitation rheology technique due to its simple experimental setup, straightforward experimental protocol, and ability to characterize samples both *in* and *ex vivo*.[2–5] NIC is performed by inserting a needle into a sample beyond the puncture point and then injecting a fluid into the sample. Upon reaching a critical pressure, rapid expansion of a void at the needle tip is observed.[6] This expansion can occur through an elastic cavitation process or an inelastic fracture process, and the critical pressure at which this expansion occurs relates to both the material properties of the sample and the needle geometry.[7] Fracture is defined as the process of creating a new surface within a material through the accumulation of molecular scale structural damage. Distinguishing these two expansion mechanisms is critical when exploiting cavitation to characterize the elastic and fracture properties of a material.[7–9]

Despite the promise of NIC, distinguishing cavitation and fracture mechanisms has remained challenging, both in terms of the experimental protocols employed and understanding the structure of the materials tested. Traditional NIC protocols have largely focused on the pressurization process while leaving the needle insertion process vague, saying only that it must be embedded in the sample beyond the point of puncture. Recent work has found that this ambiguity can lead to a 10× increase in the critical injection pressure due to the presence of residual strain below the indenter tip.[6,10] It was further found that including a retraction step to pull the needle back after insertion, which leaves an open crack below the needle tip, reduced the critical injection pressure to the point where it agreed well with theoretical predictions of the critical cavitation pressure P_{Cav}.[6] P_{Cav} is connected to both the materials properties and cavity geometry and takes the form,

$$P_{Cav} = \frac{2\gamma}{R} + \frac{5}{6}E \quad (1)$$

for a Neo–Hookean material where γ is surface tension, R is initial cavity radius (set by the outer radius of the needle), and E is elastic modulus.[11,12] Note that the coefficients in eqn (1) assume a spherical geometry and past studies have shown that this is a good approximation for the NIC geometry.[6,13,14] The critical fracture pressure P_{Frac} for NIC is given by

$$P_{Frac} = \sqrt{\frac{EG_c}{\pi R}} \quad (2)$$

where G_c is the fracture energy of the sample.[15] Note that eqn (2) assumes a planar crack geometry as opposed to the penny-shaped crack geometry often employed in NIC protocols.[7,8] A planar

Polymer Science & Engineering Department, University of Massachusetts, Amherst, MA 01003, USA. E-mail: acrosby@umass.edu

† Electronic supplementary information (ESI) available. See DOI: https://doi.org/10.1039/d2sm00400c

‡ Present Address: Department of Mechanical Engineering and Department of Chemical Engineering, University of California, Santa Barbara, CA 93106.

geometry is chosen as it should be a better representation of the long slender crack left below the needle tip when NIC is performed with a retraction step.[6]

The transition between cavitation and fracture in NIC can be found by equating P_{Cav} and P_{Frac} to get,

$$\frac{G_c}{ER} = \pi\left(\frac{2\gamma}{ER} + \frac{5}{6}\right)^2. \quad (3)$$

This connects the transition to both the cavity size and two physical size scales defined as the elastocapillary length γ/E and the elastofracture length G_c/E. γ/E is a physical size scale related to the balance between surface forces and elastic forces. In NIC, γ is set by the interfacial tension between the injection fluid and sample surface and offers limited tunability. In contrast, E connects to material structure and has a wide range of accessible values making γ/E most easily tuned by altering E.

G_c/E is a physical size scale related to the breakdown of linear elastic fracture mechanics (LEFM) and the onset of nonlinear failure mechanisms, such as crack blunting.[17] G_c/E is determined by two properties which relate to the molecular scale structure of crosslinked networks. This connection to molecular scale structure presents a challenge as most crosslinking strategies form heterogeneous networks with poorly defined structure.[18] This poor understanding of network structure has limited the experimental design of literature studies aimed at probing this transition with NIC to focus solely on tuning E instead of G_c/E as a primary variable, even though eqn (3) indicates that G_c/E is the important parameter.[7–9]

Recently, the elastic and fracture properties of model end-linked tetrafunctional poly(ethylene glycol) gels (PEG gels) were characterized.[16,19,20] Material properties of these well-defined networks were found to quantitatively agree with molecular models of elasticity and fracture, demonstrating that chain scission provided the only significant energy dissipation observed during fracture.[16] This understanding of the observed energy dissipation mechanism enables the connection between macroscopically observed deformation and molecular scale network structure. Independent characterization of both E and G_c in these model PEG gels also enables the rational design of experiments that tune G_c/E. Here, we use NIC measurements on model PEG gels, which systematically vary G_c/E, to provide new insight into the transition between cavitation and fracture mechanisms.

This work experimentally links cavitation and fracture to molecular scale structural damage by performing NIC on model PEG gels. Experimental details on the methods and materials used in this study, including a discussion of strategies for tuning the elastofracture length, are first presented. NIC measurements on the model PEG gels are then presented. Morphology of the cavities during and after expansion as well as quantitative comparison between cavitation and fracture pressure predictions are used to connect the observed expansion mechanism to molecular scale structural damage. This connection is used to rationally tune between the cavitation and fracture driven expansion mechanisms. These findings have broad implications for applications in materials characterization,[7–9] design of pressure sensitive adhesives,[21–23] and damage of biological tissues.[1,24]

2 Experimental

2.1 Methods

Full details on the experimental equipment and methods used in NIC have been recently published.[6] Here, only the details necessary for recreating these measurements are reported. NIC was performed using a needle displacement rate of 1 mm s^{-1}, maximum displacement of 15 mm, retraction distance of 7.5 mm, and volumetric compression rate of 500 microliter per minute with air as the injection fluid. Approximately 2 mL of compressible volume was contained in the system. Needle size was varied with values of the inner and outer radius (R_{in}, R_{out}) = {(80,156),(130,232),(534,737)} μm. Here, the outer radius sets the relevant size scale and is simply referred to as R in the rest of this work. Critical pressures were typically observed 30–60 s after pressurization occurred. Estimating the onset of the instability-like expansion to occur at a strain of approximately 50% gives an average strain rate of approximately 0.01 s^{-1}.[8] A summary of all experimental conditions for each set of data is available in the ESI.† Compressional dynamic mechanical analysis (DMA) was performed in this work and is

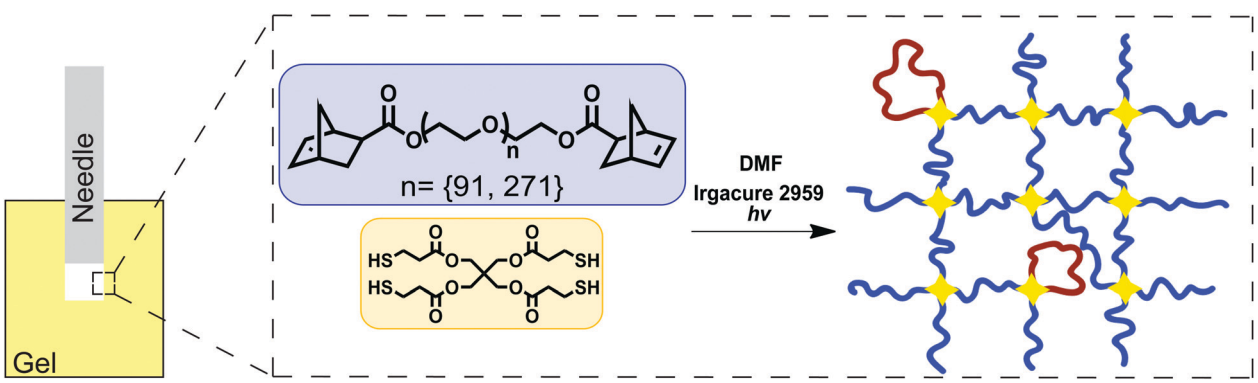

Fig. 1 Sketch showing the experimental geometry and network chemistry used in this work. This is the same synthetic approach employed recently to demonstrate a strong connection between molecular structure and both E and G_c.[16]

reported in the ESI.† The experimental notch test data presented in this work is taken from a previous publication.[16]

2.2 Materials

Tetrafunctional poly(ethylene glycol) (PEG) gels were formed in dimethylformamide (DMF) through reaction of linear telechelic PEG macromonomers with a tetrafunctional crosslinking agent (Fig. 1). Samples were tested as made without further swelling or solvent exchange. Here, only the details necessary for recreating these gels are reported. Full details on the experimental materials used in this study have been recently published.[16] Gels were synthesized using 4 kg mol^{-1} (degree of polymerization $N = 91$) and 12 kg mol^{-1} ($N = 273$) linear PEG chains at a concentration of 50 mg mL^{-1} and 77 mg mL^{-1} in DMF respectively. The end-linking strategy used to create these networks is more controlled than other strategies such as free radical polymerization or typical rubber vulcanization processes.[25–27] The structure of these gels, including the fraction of loop defects, has been characterized and reported separately.[16,20,28–31] Since the network structure of these end-linked gels is well-defined, N can be calculated from the input length of the PEG chains[16,31] and not inferred from measurements of E as is typically done for networks that have ill-defined structure.[26,32,33]

3 Tuning the elastofracture length

Probing the cavitation to fracture transition in NIC requires the ability to rationally tune G_c/E relative to the needle radius R. This presents a particular challenge as G_c and E are materials properties that lack a deterministic link at the continuum level. This means that any theoretical link between G_c and E must necessarily relate both properties to material structure. Recently, it has been shown that E in these gels is well-modeled with the real elastic network theory (RENT) model,

$$E_{\mathrm{RENT}} = 3\nu k_b T \left(\frac{\phi_o^{\frac{1}{3}} R_{ee,o}}{\phi^{\frac{1}{3}} R_{ee}} \right)^2 \left(\frac{F_{\mathrm{eff}} - 2}{F_{\mathrm{eff}}} \right) \quad (4)$$

where ν is the chain density, k_b is Boltzmann's constant, T is temperature, ϕ is polymer volume fraction, R_{ee} is the end-to-end chain distance, and F_{eff} is the effective junction functionality.[16,31] ϕ_o and $R_{ee,o}$ refer to quantities taken in the reference state, which is assumed to be at reaction conditions. It has also been shown that a loop-modified form of Lake–Thomas Theory is an appropriate description of G_c in these gels,

$$G_{c,\mathrm{RENT}} = \nu R_{ee,o} N U \left(\frac{F_{\mathrm{eff}}}{F_{\mathrm{eff}} - 2} \right)^{\frac{1}{2}} \quad (5)$$

where U is the energy released per monomer segment.[16,34] Combining these two models and assuming that $\phi = \phi_o$ (ESI†) gives,

$$\frac{G_c}{E} \sim N^{\frac{3}{2}} \phi_o^{-\frac{1}{8}} \left(\frac{F_{\mathrm{eff}}}{F_{\mathrm{eff}} - 2} \right)^{\frac{3}{2}} \quad (6)$$

predicting that while G_c/E is a strong function of N, it is a relatively weak function of ϕ_o. This suggests that if one wishes to tune G_c/E, it is best to change the molecular weight between crosslinks. However, if one wished to hold G_c/E approximately constant as E was altered, then it would be best to alter the polymer concentration.

Data showing G_c/E measured *via* pure shear notch tests performed on PEG gels at various N and ϕ_o are shown in Fig. 2.[16] Good agreement is observed between the scalings from these plots and those predicted by eqn (6). Note that while the range of ϕ_o values accessed here is not wide enough to distinguish between a ϕ_o^{0} and $\phi_o^{-\frac{1}{8}}$ scaling, it is clear from the

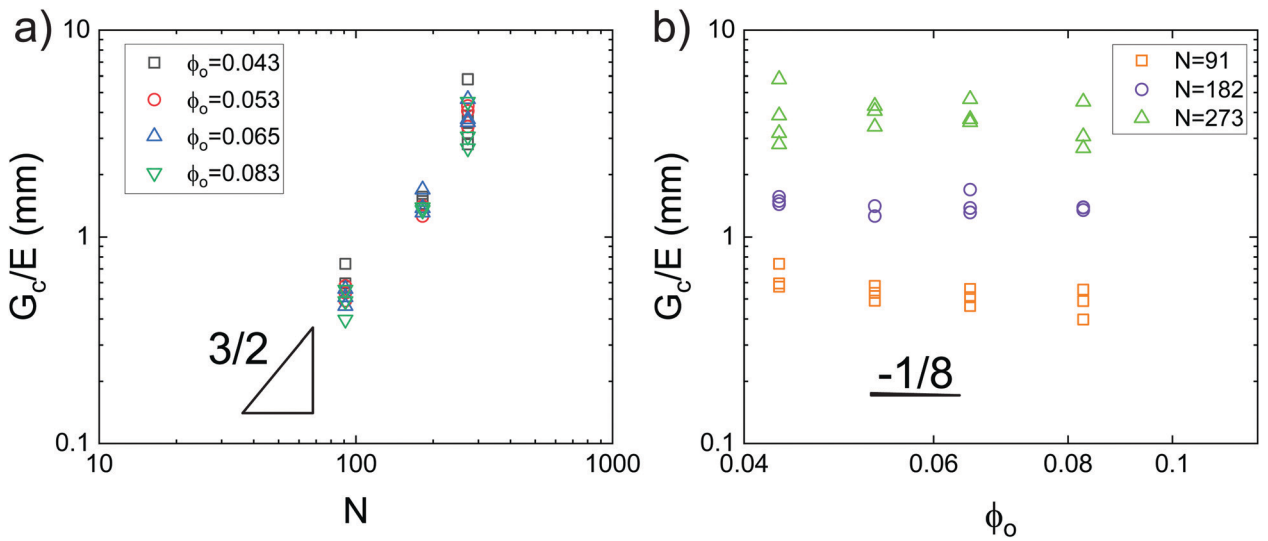

Fig. 2 Plots of the elastofracture length against (a) N and (b) ϕ_o showing strong agreement with the scaling predictions of eqn (6). Data is taken from pure shear notch tests.[16] Agreement between the data and theoretical scalings shows that altering N is a more effective means of tuning G_c/E.

data that $\frac{G_c}{E}$ does not vary significantly over the ϕ_o range used in the NIC experiments. This agreement confirms that altering N is an effective means of tuning G_c/E while altering ϕ_o is not. This means that while both ϕ_o and N are altered between samples used in this study, tuning N is the underlying change which drives a shift in G_c/E. These results highlight the importance of understanding the coupled nature of G_c and E when designing experiments around tuning the elastofracture length.

4 Needle-induced cavitation of model gels

The transition between cavitation and fracture mechanisms is related to the needle size R and both γ/E and G_c/E, as laid out in eqn (3). Assuming that $\gamma \approx 40$ mN m^{-1} and $E \approx 10$ kPa gives an estimate of γ/E on the order of 10^{-6} m. Taking the ratio of γ/E relative to the smallest needle size $R \approx 10^{-4}$ m, gives a value of approximately 0.01 which is negligible compared to the 5/6 value in eqn (3). Since the contribution from interfacial tension is negligible, the crossover point between P_{Cav} and P_{Frac} is predicted at a value of RE/G_c = 0.46. Images of the cavity at the needle tip starting at the onset of expansion and increasing with time as a function of R normalized by G_c/E are shown in Fig. 3. Videos SV1–4 (ESI†) show the full runs for RE/G_c = {0.84,0.37,0.27,0.02}, respectively. Note that the optical contrast of the roughness at the cavity surface is influenced by the orientation of the crack. Since this is randomly determined by the needle insertion process and does not become apparent until expansion occurs, all discussion of roughness in this work is qualitative. RE/G_c is adjusted from 0.84 to 0.27 by altering the size of the needle employed. RE/G_c is shifted from 0.27 to 0.02 by tuning G_c/E.

The morphologies observed in these images display four potential expansion mechanisms. When RE/G_c = 0.84, the cavity at the start and finish of expansion is rough and lacks axisymmetry indicating a fracture process driving expansion. This leads to the rupture of network chains at the crack tip. When RE/G_c = 0.37 and RE/G_c = 0.27, the cavity at the start of expansion is smooth, and then transitions to being rough indicating a cavitation-initiated expansion that transitions to a fracture process. This also leads to the rupture of network chains at the crack tip. When RE/G_c = 0.02, the cavity at the start and finish of expansion is smooth which suggests either an elastic cavitation process or an inelastic cavitation process where damage occurs in the material through a nonlinear failure mechanism. These results indicate that visualization of the cavity at the start and finish of the expansion can be used to distinguish between all expansion mechanisms except for those where expansion of the cavity stabilizes before the ultimate failure stretch is achieved.

While the expansion when RE/G_c = 0.02 appears similar to a purely elastic cavitation process, visual measurements alone cannot determine that irreversible changes, or damage, do not occur to the network. This potential damage is sketched in Fig. 3 as being localized around the crack tip as one might expect during blunted crack propagation;[17] however, recent experimental work suggests that the damage may be more distributed in this case.[35] The images in Fig. 3 can be used to distinguish whether or not damage must occur by calculating the volumetric stretch at the cavity surface after expansion.

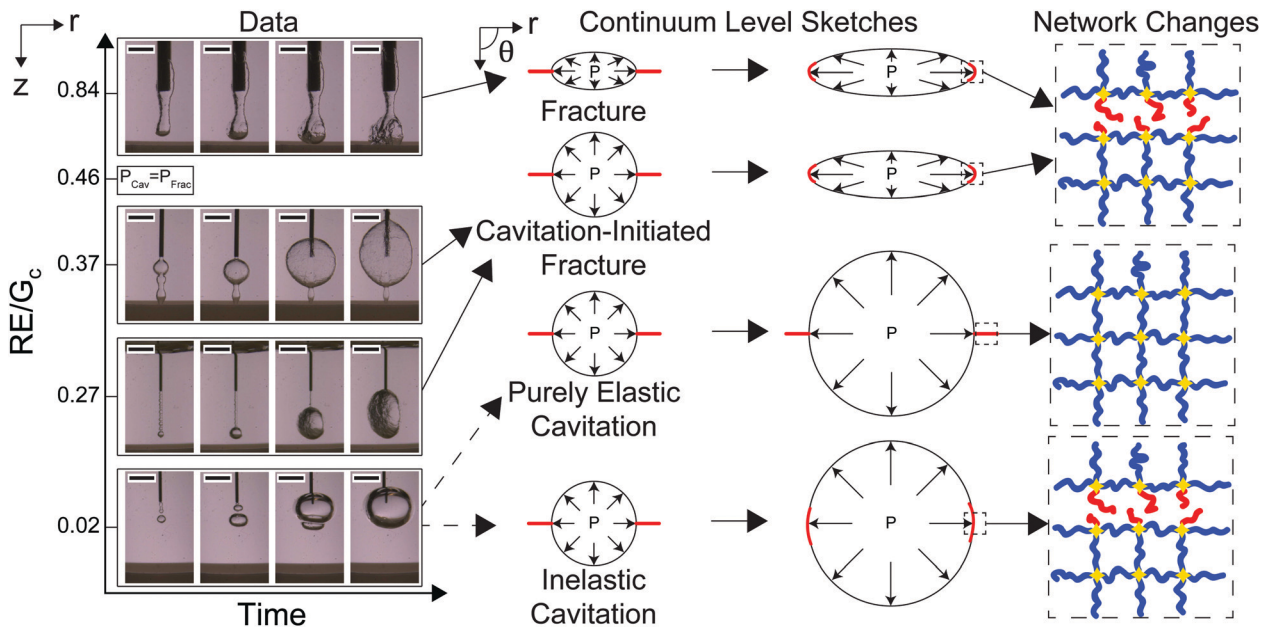

Fig. 3 Images of the cavity starting at the critical pressure and increasing with time as a function of RE/G_c. Sketches of the process from a continuum perspective and molecular perspective are also shown. Note that the sketches shown are in a different viewing plane than the one shown in the experimental images. The red lines in the continuum level sketches represent the potential crack path that would open up if crack propagation were to occur. When RE/G_c = 0.02 two potential expansion mechanisms are observed. Scale bars are 2.5 mm in length.

Taking the square root of the ratio between the final and initial surface area A between the surfaces at the start and finish of expansion can then be use to estimate the maximum stretch λ_{max},

$$\lambda_{max} = \left(\frac{A}{A_o}\right)^{\frac{1}{2}} = \sqrt{\frac{4\pi r^2}{2\pi Rl}} \quad (7)$$

where r is the radius of the cavity in the fully expanded state, and l is the axial length of the void below the needle tip modeled here as a cylinder. As seen in Fig. 3, the cavity is not perfectly spherical. Estimating the radius of the cavity in the axial and radial directions gives radii of 2.17 mm and 2.69 mm, respectively. The radius of the initial tubular defect is estimated to be 0.156 mm and the height is measured as 2.1 mm. These calculations give estimates of λ_{max} = 5.4 or λ_{max} = 6.6 at the surface of the material when using the cavity radius estimate in the axial and radial directions, respectively. Due to the shape of the cavity, λ_{max} = 5.4 is an underestimate of the stretch and λ_{max} = 6.6 is an overestimate. The maximum stretch a network chain can undergo can then be used to estimate whether or not the material could accommodate the observed deformation without damaging the network structure. Assuming uniaxial extension, $\lambda_1 = \lambda$, thus $\lambda_2 = \lambda_3 = \lambda^{-1/2}$ through an assumption of incompressibility. λ_{max} in the wet state can be estimated using the unconstrained end-to-end distance of a network chain $R_{ee,o}$ and its contour length $R_{ee,max}$,

$$\lambda_{max,wet} = \left(\frac{R_{ee,max}}{\lambda_s R_{ee,o}}\right) = \phi^{\frac{1}{3}}\sqrt{\frac{V_{PEG}}{V_{Ref}}N} = 5.5, \quad (8)$$

as developed and validated against data from Akagi *et al.*[36] in the ESI,† where λ_s is a swelling ratio, V_{PEG} = 0.069 nm^3 is PEG monomer volume, and V_{Ref} = 0.1 nm^3 is the monomer reference volume. These calculations show a maximum volumetric stretch that can be accommodated of $\lambda_{max,wet}$ = 5.5. This value is only 1.8% higher than our lower bound value, which represents an underestimate of the strain in the system, of λ_{max} = 5.4. Based on this, we conclude that some damage to the molecular structure must occur to reach the stretch values observed in experiment when RE/G_c = 0.02. This result suggests that an inelastic cavitation mechanism is observed here, where expansion is initiated by an elastic cavitation process and inelastic damage develops through some nonlinear failure process during expansion. However, in this case the cavity remains smooth and spherical since the final pressure at which the stretch stabilizes is greater than P_{Cav}.

While the cavity morphology can be used to distinguish between the expansion mechanisms, these phenomena are also distinguishable through quantitative predictions of the cavitation and fracture pressures. Experimentally observed critical pressure P_c normalized by P_{Cav} plotted against RE/G_c is shown in Fig. 4a. The solid black line represents P_{Frac}/P_{Cav} with negligible interfacial tension and the arrows show the crossover point where RE/G_c = 0.46. At low values of RE/G_c, $P_c/P_{Cav} \ll P_{Frac}/P_{Cav}$ indicating that the threshold cavitation pressure is realized well below the criterion for fracture in support of the inelastic cavitation mechanism proposed above. The divergence of P_{Frac}/P_{Cav} as RE/$G_c \rightarrow 0$ shows that the inelastic cavitation mechanism is made possible by a breakdown of LEFM, which is often assumed to hold when modeling the transition between cavitation and fracture.[8] At intermediate values of RE/G_c, $P_c/P_{Cav} < P_{Frac}/P_{Cav}$ indicating that the cavitation pressure is near but less than the fracture pressure. This finding indicates that initiation of expansion will occur through an elastic cavitation mechanism; however, the fracture criterion will be satisfied during expansion resulting in a cavitation-initiated fracture mechanism. At large values of RE/G_c, $P_c/P_{Cav} > P_{Frac}/P_{Cav}$ indicating that the fracture pressure will

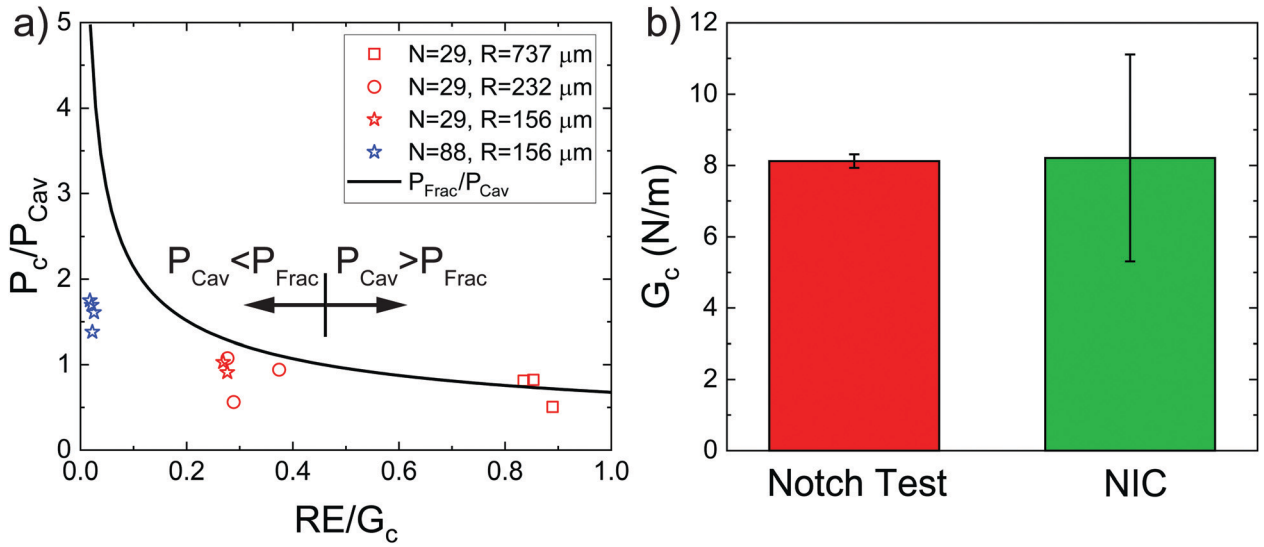

Fig. 4 (a) Plot of the experimentally observed critical expansion pressure P_c normalized by P_{Cav} against RE/G_c. The black line represents the point at which fracture is predicted to occur. (b) Plot showing the comparison between G_c measured with notch tests by Barney *et al.*[16] and measured with NIC in this work when RE/$G_c \approx 0.84$.

be realized before the cavitation pressure leading to a straightforward fracture expansion mechanism. Also note that the measurements at $RE/G_c \approx 0.84$ provide the first experimental verification that G_c measured with NIC agrees with an independent estimate from notch tests as shown in Fig. 4b.[16]

The results presented above indicate that previously developed theory[8] was able to predict the expansion mechanism in all cases except for when $RE/G_c = 0.02$. Expansion under these conditions ($RE/G_c = 0.02$) was predicted to be a purely elastic cavitation mechanism; however an inelastic cavitation mechanism resulting in damage was observed. This difference is most likely due to the assumption that crack propagation in these cases can be modeled using LEFM; however, cavitation of the void coincides with the onset of extreme blunting at the crack tip.[8,37] Kang *et al.* have provided some modeling of blunted systems and found that distinguishing between purely elastic cavitation and inelastic cavitation where damage occurs at the blunted crack tip is non-trivial.[38] In this study, it was only possible through the use of materials with well-defined network structure. This shows that cavitation processes that may appear to be elastic at a macroscopic level can still damage the underlying material structure.

While the results presented above demonstrate that the cavitation to fraction transition can be readily tuned by altering G_c/E relative to the cavity geometry, it is important to discuss the limitations of our findings. First, NIC relies on the needle insertion process to define the initial crack geometry. This process damages the material and can often lead to crack morphologies more complex than those reported here.[39] Further investigation into what causes more complex crack morphologies during puncture and how that impacts the NIC response is of interest in the future. Second, NIC is a technique where the expansion mechanism relates to both G_c/E and γ/E; however, this work only operates in the limit where γ/E is negligible. The quantitative impact of interfacial energies on the transition from cavitation to fracture remains an open question where further experimental data would provide clarity. Third, while there is a clearly defined theoretical and experimental boundary between fracture and cavitation-initiated fracture mechanisms, no boundaries are drawn between cavitation-initiated fracture, purely elastic cavitation, and inelastic cavitation. Probing these boundaries is of interest in the future and will likely require consideration of further experimental variables, such as the amount of compressible air contained in the pressure system.[8,40] Finally, while it was shown that some structural damage must occur to accommodate the deformations observed when $RE/G_c = 0.02$, the way in which this nonlinear damage proceeds is not addressed by this work.

5 Conclusions

Recent improvements in needle-induced cavitation and a quantitative link between network structure and the elastic and fracture properties of a set of model end-linked PEG gels were exploited to experimentally connect cavitation and fracture to molecular scale damage. These results indicated that damage may still occur when a macroscopically smooth cavitation event is observed. It was also experimentally confirmed that measurements of fracture energy from NIC measurements agreed with those from notch tests.

Conflicts of interest

The authors declare no conflicts of interest.

Acknowledgements

The authors acknowledge funding support from the Office of Naval Research (ONR grant number N00014-17-1-2056). The authors would also like to thank Professor Robert A. Riggleman for helpful discussions about estimating the maximum attainable stretch in our networks.

References

1 C. W. Barney, C. E. Dougan, K. R. Mcleod, A. Kazemimoridani, Y. Zheng, Z. Ye, S. Tiwari, I. Sacligil, R. A. Riggleman, S. Cai, J.-H. Lee, S. R. Peyton, G. N. Tew and A. J. Crosby, *Proc. Natl. Acad. Sci. U. S. A.*, 2020, **117**, 9157–9165.
2 J. A. Zimberlin, N. Sanabria-DeLong, G. N. Tew and A. J. Crosby, *Soft Matter*, 2007, **3**, 763.
3 J. A. Zimberlin, J. J. McManus and A. J. Crosby, *Soft Matter*, 2010, **6**, 3632.
4 J. Cui, C. H. Lee, A. Delbos, J. J. McManus and A. J. Crosby, *Soft Matter*, 2011, **7**, 7827.
5 L. E. Jansen, N. P. Birch, J. D. Schiffman, A. J. Crosby and S. R. Peyton, *J. Mech. Behav. Biomed. Mater.*, 2015, **50**, 299–307.
6 C. W. Barney, Y. Zheng, S. Wu, S. Cai and A. J. Crosby, *Soft Matter*, 2019, **15**, 7390–7397.
7 S. Kundu and A. J. Crosby, *Soft Matter*, 2009, **5**, 3963.
8 S. B. Hutchens, S. Fakhouri and A. J. Crosby, *Soft Matter*, 2016, **12**, 2557–2566.
9 S. Raayai-Ardakani, D. R. Earl and T. Cohen, *Soft Matter*, 2019, 4999–5005.
10 C. W. Barney, C. Chen and A. J. Crosby, *Soft Matter*, 2021, **17**, 5574–5580.
11 A. N. Gent and P. B. Lindley, *Proc. R. Soc. London, Ser. A*, 1959, **249**, 195–205.
12 A. N. Gent and D.-a Tompkins, *Rubber Chem. Technol.*, 1970, **43**, 873–877.
13 S. B. Hutchens and A. J. Crosby, *Soft Matter*, 2014, **10**, 3679–3684.
14 S. Raayai-Ardakani, Z. Chen, D. R. Earl and T. Cohen, *Soft Matter*, 2018, **15**, 381–392.
15 A. A. Griffith, *Philos. Trans. R. Soc., A*, 1921, **221**, 163–198.

16 C. W. Barney, Z. Ye, I. Sacligil, K. R. Mcleod, H. Zhang, G. N. Tew, R. A. Riggleman and A. J. Crosby, *Proc. Natl. Acad. Sci. U. S. A.*, 2022, **119**, 1–6.
17 C.-Y. Hui, A. Jagota, S. J. Bennison and J. D. Londono, *Proc. R. Soc. London, Ser. A*, 2003, **459**, 1489–1516.
18 S. Seiffert, *Polym. Chem.*, 2017, **3**, 4472–4487.
19 J. Cui, M. A. Lackey, G. N. Tew and A. J. Crosby, *Macromolecules*, 2012, **45**, 6104–6110.
20 E. M. Saffer, M. A. Lackey, D. M. Griffin, S. Kishore, G. N. Tew and S. R. Bhatia, *Soft Matter*, 2014, **10**, 1905.
21 C. Creton and M. Ciccotti, *Rep. Prog. Phys.*, 2016, **79**, 046601.
22 A. J. Crosby, K. R. Shull, H. Lakrout and C. Creton, *J. Appl. Phys.*, 2000, **88**, 2956–2966.
23 H. Lakrout, P. Sergot and C. Creton, *J. Adhes.*, 1999, **69**, 307–359.
24 Y. Kurosawa, K. Kato, S. Saito, M. Kubo, T. Uzuka, Y. Fujii and H. Takahashi, *Conf. Proc. IEEE Eng. Med. Biol. Soc.*, 2009, 7224–7227.
25 M. Malkoch, R. Vestberg, N. Gupta, L. Mespouille, P. Dubois, A. F. Mason, J. L. Hedrick, Q. Liao, C. W. Frank, K. Kingsbury and C. J. Hawker, *Chem. Commun.*, 2006, 2774–2776.
26 P. J. Flory, *Chem. Rev.*, 1944, **35**, 51–75.
27 S. Lin-Gibson, R. L. Jones, N. R. Washburn and F. Horkay, *Macromolecules*, 2005, **38**, 2897–2902.
28 T. Sakai, T. Matsunaga, Y. Yamamoto, C. Ito, R. Yoshida, S. Suzuki, N. Sasaki, M. Shibayama and U.-I. Chung, *Macromolecules*, 2008, **41**, 5379–5384.
29 K. Kawamoto, M. Zhong, R. Wang, B. D. Olsen and J. A. Johnson, *Macromolecules*, 2015, **48**, 8980–8988.
30 R. Wang, A. Alexander-Katz, J. A. Johnson and B. D. Olsen, *Phys. Rev. Lett.*, 2016, **116**, 1–5.
31 M. Zhong, R. Wang, K. Kawamoto, B. D. Olsen and J. A. Johnson, *Science*, 2016, **353**, 1264–1268.
32 C. Yang, T. Yin and Z. Suo, *J. Mech. Phys. Solids*, 2019, **131**, 43–55.
33 S. P. Obukhov, M. Rubinstein and R. H. Colby, *Macromolecules*, 1994, **27**, 3191–3198.
34 G. J. Lake and A. G. Thomas, *Proc. R. Soc. London, Ser. A*, 1967, **300**, 108–119.
35 J. Y. Kim, Z. Liu, B. M. Weon, T. Cohen, C.-Y. Hui, E. R. Dufresne and R. W. Style, *Sci. Adv.*, 2020, **6**, 1–7.
36 Y. Akagi, T. Katashima, H. Sakurai, U. I. Chung and T. Sakai, *RSC Adv.*, 2013, **3**, 13251–13258.
37 Z. Song and S. Cai, *Extreme Mech. Lett.*, 2022, 101673.
38 J. Kang, C. Wang and S. Cai, *Soft Matter*, 2017, **13**, 6372–6376.
39 W.-c Lin, K. J. Otim, J. L. Lenhart, P. J. Cole and K. R. Shull, *J. Mater. Res.*, 2009, **24**, 957–965.
40 A. Delbos, J. Cui, S. Fakhouri and A. J. Crosby, *Soft Matter*, 2012, **8**, 8204.

